The Astrophysical Journal, 568:743–753, 2002 April 1

COLLAPSE AND FRAGMENTATION OF MOLECULAR CLOUD CORES. VII. MAGNETIC FIELDS AND MULTIPLE PROTOSTAR FORMATION

Alan P. Boss
Department of Terrestrial Magnetism, Carnegie Institution of Washington, 5241 Broad Branch Road, NW, Washington, DC 20015-1305; boss@dtm.ciw.edu
Received 2001 October 16; accepted 2001 December 6

ABSTRACT

Recent observations of star-forming regions suggest that binary and multiple young stars are the rule rather than the exception and implicate fragmentation as the likely mechanism for their formation. Most numerical hydrodynamic calculations of fragmentation have neglected the possibly deleterious effects of magnetic fields, despite ample evidence for the importance of magnetic support of precollapse clouds. We present here the first numerical hydrodynamic survey of the collapse and fragmentation of initially magnetically supported clouds that takes into account several magnetic field effects in an approximate manner. The models are calculated with a three-dimensional, finite differences code that solves the equations of hydrodynamics, gravitation, and radiative transfer in the Eddington and diffusion approximations. Magnetic field effects are included through two simple approximations: magnetic pressure is added to the gas pressure, and magnetic tension is approximated by gravity dilution once collapse is well underway. Ambipolar diffusion of the magnetic field leading to cloud collapse is treated approximately as well. Models are calculated for a variety of initial cloud density profiles, shapes, and rotation rates. We find that in spite of the inclusion of magnetic field effects, dense cloud cores are capable of fragmenting into binary and multiple protostar systems. Initially prolate clouds tend to fragment into binary protostars, while initially oblate clouds tend to fragment into multiple protostar systems containing a small number (of the order of 4) of fragments. The latter are likely to be subject to rapid orbital evolution, with close encounters possibly leading to the ejection of fragments. Contrary to expectation, magnetic tension effects appear to enhance fragmentation, allowing lower mass fragments to form than would otherwise be possible, because magnetic tension helps to prevent a central density singularity from forming and producing a dominant single object. Magnetically supported dense cloud cores thus seem to be capable of collapsing and fragmenting into sufficient numbers of binary and multiple protostar systems to be compatible with observations of the relative rarity of single protostars.

Subject headings: binaries: general — hydrodynamics — ISM: clouds — ISM: kinematics and dynamics — MHD — stars: formation

1. INTRODUCTION

Classical theories of binary star formation assume that stars form singly and then either fission into two bodies or else are captured or otherwise end up in orbit around one another, in order to explain the frequent occurrence of binary main-sequence (Duquennoy & Mayor 1991; Fischer & Marcy 1992) and pre–main-sequence stars (Mathieu 1994; Ghez et al. 1997). There is an emerging viewpoint, however, that single protostars may not be the fundamental building block of binary star systems. Rather, the idea has been proposed that protostars may form preferentially in binary and multiple systems, with the orbital disruption of these systems leading to the ejection of single protostars (Larson 1995; Sterzik & Durisen 1998; Reipurth 2000; Reipurth & Clarke 2001). The validity of this novel viewpoint about star formation depends upon having a robust mechanism for producing binary and multiple protostars, such as fragmentation, defined to be the breakup of molecular cloud cores during their collapse to become protostars.

Evidence for the presence of binary and multiple objects at the earliest observable phases of the star formation process (e.g., Fuller, Ladd, & Hodapp 1996) has continued to mount. T Tauri, the prototypical pre–main-sequence star, is now believed to be a triple system (Koresko 2000) and may even be a quintuple. Gliese 569B may be a young, triple brown dwarf system (Kenworthy et al. 2001). The binary frequency among the pre–main-sequence stars in the Scorpius-Centaurus OB association is *higher* than that for main-sequence stars for a wide range of separations (Köhler et al. 2000). L1551 IRS 5, the prototypical bipolar outflow source, is now known to be a binary (Rodríguez et al. 1998), as is its close neighbor, the L1551NE protostar (Moriarty-Schieven et al. 2000). A binary protostar has been found in the Bok globule BHR 71 (Bourke 2001). The WL 20 triple system, consisting of two T Tauri stars and an embedded protostar, is so compact as to be orbitally unstable (Ressler & Barsony 2001). The NGC 1333/IRAS 4 triple protostar system is similarly orbitally unstable (Smith et al. 2000) and will undergo close encounters. Fragmentation of collapsing clouds seems to be required to explain the wide range in orbital periods of binary stars (Kroupa & Burkert 2001). These and other observational constraints strongly imply that fragmentation is the dominant mechanism for binary and multiple-star formation (White & Ghez 2001).

Fragmentation thus appears to be the desired robust mechanism for forming binary and multiple protostars (reviewed by Bodenheimer et al. 2000). Observations have also shown, however, that molecular cloud cores appear to be supported against collapse largely by magnetic fields (Crutcher 1999). Most protostellar fragmentation calculations have either ignored the effects of magnetic fields or have found that in the presence of frozen-in magnetic fields, little contraction occurs, thus preventing fragmentation

(Dorfi 1982; Benz 1984), or else that collapse occurs but fragmentation does not (Phillips 1986a, 1986b). As discussed in Boss (1997), the latter result may be caused in part by the lack of rotation in Phillips's models: even in the absence of magnetic fields and thermal pressure, the Phillips (1986a) models did not lead to robust fragmentation. Given this situation, it is prudent to reconsider the role of magnetic fields in fragmentation calculations.

The standard theory of star formation (Shu, Adams, & Lizano 1987) hypothesizes that molecular cloud cores are largely magnetically supported and contract as a result of loss of magnetic field support caused by ambipolar diffusion of the neutral atoms inward through the ions. Models of the growth of nonaxisymmetry in magnetized equilibrium disks imply that fission cannot occur (Galli et al. 2001), suggesting that rapid loss of magnetic flux during gravitational collapse is needed in order to form binary and multiple stars. Axisymmetric models of ambipolar diffusion imply that a magnetically subcritical, nonrotating cloud can contract to form a magnetically supercritical ring, which might then fragment into multiple objects in a nonaxisymmetric calculation (Li 2001).

Previous nonaxisymmetric calculations of the collapse of magnetic prolate cloud cores starting from Gaussian density profiles found that cores with sufficiently rapid initial rotation rates fragmented into binary protostars, whereas clouds with slower rotation formed only bars or single protostars (Boss 1997, 1999). These models included only the effect of magnetic pressure and not of magnetic tension, which effectively dilutes self-gravitational forces once collapse proceeds and a thin disk forms (Basu 1997; Shu & Li 1997). Because self-gravity is the force that ultimately drives fragmentation, the obvious concern is that magnetic tension could prevent fragmentation altogether or perhaps limit the region of parameter space in which fragmentation occurs to a subset of the region permitted for clouds with significant rotation (Boss 1997, 1999).

We present here the first survey of three-dimensional models of the collapse of initially magnetically supported clouds, taking into account magnetic field pressure as well as magnetic tension forces through the gravity dilution approximation. The results of a few of these models have been previously reported (Boss 2000, 2001), but the entire suite of models, exploring the effects of variations in a cloud core's initial density profile, shape, and rotation rate, is described here. We will see that, contrary to expectations, magnetic tension seems to have a salubrious effect regarding fragmentation, even for slowly rotating clouds.

2. NUMERICAL METHODS

The numerical models are calculated with a three-dimensional hydrodynamics code that calculates finite-difference solutions of the equations of radiative transfer, hydrodynamics, and gravitation for an inviscid gas (Boss & Myhill 1992). The hydrodynamic equations are solved in conservation-law form on a contracting spherical coordinate grid, subject to constant volume boundary conditions on the spherical boundary. The code is second-order accurate in both space and time, and the van Leer–type hydrodynamic fluxes have been modified to improve stability (Boss 1997). Artificial viscosity is not employed. The code has been tested extensively on a variety of test problems (Boss & Myhill 1992), including both the standard isothermal test case and the standard nonisothermal test case (Myhill & Boss 1993).

The Poisson equation for the cloud's gravitational potential is solved by a spherical harmonic expansion (Y_{lm}) including terms up to $N_{lm} = 16$. The computational grid consists of a spherical coordinate grid with $N_r = 200$, $N_\theta = 22$ for $\pi/2 \geq \theta \geq 0$ (symmetry through the midplane is assumed for $\pi \geq \theta > \pi/2$), and $N_\phi = 64$ or 128. For these models, the active ϕ grid is restricted to the range $\pi \geq \phi \geq 0$, with symmetry through the rotational axis being assumed for $2\pi \geq \phi > \pi$ in order to double the ϕ resolution with less computational cost. In these "π symmetry" models, only even m modes can grow. The radial grid contracts to follow the collapsing inner regions and to provide sufficient spatial resolution to ensure satisfaction of the four Jeans conditions for a spherical coordinate grid (Truelove et al. 1997; Boss et al. 2000). For some models, a variation on the usual radial grid is employed, in which the innermost 50 radial grid points are kept uniformly spaced during grid contraction, while the outermost 150 are nonuniformly spaced, in order to provide an inner region with uniform spatial resolution. The ϕ grid is always uniformly spaced, whereas the θ grid is compressed toward the midplane, where the minimum grid spacing is 0.°3.

3. RADIATIVE TRANSFER

Radiative transfer is handled in the Eddington or diffusion approximations, including detailed equations of state and dust grain opacities (Boss & Myhill 1992). In the Eddington approximation, the hydrodynamic equations are supplemented by the energy equation

$$\frac{\partial(\rho E)}{\partial t} + \nabla \cdot (\rho E \boldsymbol{v}) = -p \nabla \cdot \boldsymbol{v} + L \, ,$$

where ρ is the gas density, $\boldsymbol{v}$ is the fluid velocity, E is the specific internal energy [$E = E(\rho, \ T)$, where T is the gas and dust temperature], p is the gas pressure [$p = p(\rho, \ T)$], and L is the rate of change of internal energy due to radiative transfer. The energy equation is solved explicitly in conservation-law form, as are the other four hydrodynamic equations.

The formulation of L depends on the optical depth τ:

$$L = 4\pi\kappa\rho(J - \hat{\boldsymbol{B}}) \, , \quad \tau < \tau_c \, ,$$

$$L = \frac{4\pi}{3} \nabla \cdot \left(\frac{1}{\kappa\rho} \nabla J \right) , \quad \tau > \tau_c \, ,$$

where τ_c is a critical value for the optical depth ($\tau_c = 10$ in these models), κ is the Rosseland mean opacity of the gas and dust, J is the mean intensity, and $\hat{\boldsymbol{B}} = \sigma T^4/\pi$ is the Planck function. The mean intensity is determined by the equation

$$\frac{1}{3} \frac{1}{\kappa\rho} \nabla \cdot \left(\frac{1}{\kappa\rho} \nabla J \right) - J = -\hat{\boldsymbol{B}} \, .$$

The Eddington approximation is used during the initial phases of collapse, before the centers of the clouds become very optically thick. Once collapse is well underway and central densities have exceeded $\sim 10^{-11}$ g cm^{-3}, however, the iterative solution for the mean intensity becomes prohibitively slow. At this point, the Eddington approximation is replaced by the diffusion approximation. Because of the

high optical depths at the cloud centers ($\tau > 10^3$) by this phase, the diffusion approximation is valid, and the diffusion approximation imposes little added computational burden.

In the diffusion approximation, the energy equation is solved in the form

$$\frac{\partial(\rho E)}{\partial t} + \nabla \cdot (\rho E \boldsymbol{v}) = -p\nabla \cdot \boldsymbol{v} + \nabla \cdot \left[\frac{4}{3\kappa\rho}\nabla(\sigma T^4)\right] ,$$

where σ is the Stefan-Boltzmann constant ($\sigma = 5.67 \times 10^{-5}$ cgs). The radiative flux term is set equal to zero in regions where the optical depth τ drops below 10 in order to ensure that the diffusion approximation does not affect the solution in regions of low optical depth where it is not strictly valid.

4. MAGNETIC FIELD APPROXIMATIONS

The problem of fragmentation in a magnetic cloud core subject to ambipolar diffusion deserves to be studied with a true magnetohydrodynamics (MHD) code, such as the ZEUS code (Stone & Norman 1992). Considerable progress can be made, however, by including the effects of magnetic fields through several reasonably good approximations. The full MHD momentum equation (Jackson 1962) is

$$\rho\frac{\partial \boldsymbol{v}}{\partial t} + \rho\boldsymbol{v} \cdot \nabla\boldsymbol{v} = -\rho\nabla\Phi - \nabla p + \frac{1}{c}(\boldsymbol{J} \times \boldsymbol{B}) ,$$

where Φ is the gravitational potential, c is the speed of light, $\boldsymbol{J}$ is the current density, and $\boldsymbol{B}$ is the magnetic field. In the limit of high electrical conductivity, as is appropriate for molecular cloud cores in spite of their low fractional ionization, Ampere's law holds, so that

$$\frac{1}{c}\boldsymbol{J} = \frac{1}{4\pi}(\nabla \times \boldsymbol{B}) .$$

The magnetic effects term can then be written as

$$\frac{1}{c}(\boldsymbol{J} \times \boldsymbol{B}) = -\nabla\left(\frac{B^2}{8\pi}\right) + \frac{1}{4\pi}(\boldsymbol{B} \cdot \nabla)\boldsymbol{B} .$$

For a straight, single-component magnetic field $\boldsymbol{B} = [0,\ 0,\ B_z(x,\ y)]$, the magnetic field tension term $(\boldsymbol{B} \cdot \nabla)\boldsymbol{B}$ vanishes, leaving

$$\frac{1}{c}(\boldsymbol{J} \times \boldsymbol{B}) = -\nabla\left(\frac{B^2}{8\pi}\right) .$$

The full MHD momentum equation then becomes

$$\rho\frac{\partial \boldsymbol{v}}{\partial t} + \rho\boldsymbol{v} \cdot \nabla\boldsymbol{v} = -\rho\nabla\Phi - \nabla\left(p + \frac{B^2}{8\pi}\right) .$$

Boss (1997) approximated the effects of magnetic fields simply by adding the effective magnetic pressure term $(B^2/8\pi)$ to the gas pressure. Calculations of the contraction of magnetic clouds constrained to axisymmetry show that initially straight magnetic field lines remain remarkably straight prior to the onset of dynamic collapse (e.g., Fiedler & Mouschovias 1993).

Once protostellar collapse is well underway, magnetic field lines will bend significantly and exert a tension force that counteracts gravity. Magnetically controlled clouds tend to contract and flatten along the magnetic field lines and to form thin disks. For a thin disk with a constant mass-to-flux ratio, the acceleration due to magnetic tension is proportional to the gravitational acceleration, greatly simplifying its inclusion in models (Basu 1997; Shu & Li 1997; Nakamura & Hanawa 1997). For a thin disk with a mass-to-flux ratio μ, the magnetic acceleration a_m can be expressed as (e.g., Basu 1997, 1998)

$$a_m = a_{\rm tension} + a_{\rm pressure} = -\frac{1}{\mu^2}g_r + \frac{2}{\mu^2}a_T ,$$

where g_r is the gravitational acceleration and a_T is the thermal acceleration. The magnetic tension acceleration $a_{\rm tension}$ can thus be written as

$$a_{\rm tension} = -\frac{1}{2}\frac{g_r}{a_T}a_{\rm pressure} = -\frac{1}{2}\nabla\Phi\frac{\nabla(B^2/8\pi)}{\nabla p} .$$

The magnetic tension acceleration can then be included simply by modifying the gravitational potential as follows:

$$\nabla\Phi \rightarrow \left[1 - \frac{1}{2}\frac{\nabla(B^2/8\pi)}{\nabla p}\right]\nabla\Phi .$$

Observationally (Crutcher 1999) and theoretically (Mouschovias 1991), the magnetic field strength depends on the density as

$$B = B_0\left(\frac{\rho}{\rho_0}\right)^{\kappa} ,$$

where $\kappa \approx \frac{1}{2}$ (see also Ostriker, Stone, & Gammie 2001). For an isothermal gas and $\kappa = \frac{1}{2}$, the gradient of the density occurs in both the numerator and denominator of the modified gravitational potential term and so cancels out, leaving

$$\frac{\nabla(B^2/8\pi)}{\nabla p} = \frac{p_{\rm mag}(t)}{p(t=0)} = f(t) .$$

Thus, once a thin magnetic disk forms, magnetic tension forces can be approximated by diluting the gravitational potential by a factor involving a function only of time:

$$\Phi \rightarrow \Phi \times \left[1 - \tfrac{1}{2}f(t)\right] ,$$

where $f(t)$ decreases with time because of the effects of ambipolar diffusion. A similar approximation was employed by Nakamura & Hanawa (1997) in their thin magnetic disk models. Ambipolar diffusion is thought to be the primary cause for rapid loss of magnetic flux in collapsing cloud cores, rather than Ohmic dissipation (Desch & Mouschovias 2001), with complete magnetic decoupling occurring for central densities in the range of $\sim 10^{-13}$ to $\sim 10^{-11}$ g cm^{-3}.

In the present models, once the central density exceeds 10^{-15} g cm^{-3}, signifying the onset of the dynamic collapse phase, the overall gravitational potential is diluted by the factor

$$\Phi \rightarrow \Phi \times \left[1 - 1.1\left(\frac{\tau_{\rm AD} - t}{\tau_{\rm AD}}\right)^2\right] ,$$

where 1.1 is a coefficient that depends on the particular choices for B_0, ρ_0, and the initial temperature used in all of these models. While this approximation strictly applies only once a thin disk is formed, magnetic tension has the same qualitative effect of opposing gravity during the collapse

phase prior to disk formation, so this approximation is also used immediately prior to disk formation. Fragmentation does not begin in these models until well after a disk has formed and the central density has exceeded $\sim 10^{-11}$ g cm^{-3}, an increase in density by a factor of $\sim 10^4$ from the initiation of gravity dilution, so the exact choice of the onset of gravity dilution should not be critical to the outcome.

The effects of ambipolar diffusion (e.g., Ciolek & Mouschovias 1995) are approximated in the new models (as well as in Boss 1997, 1999, 2000, 2001) by specifying that

$$B_0 = B_0(t) = B_{oi}\left(1 - \frac{t}{\tau_{\rm AD}}\right) ,$$

where B_{oi} is a constant equal to 200 μG, t is the model time, and the ambipolar diffusion timescale $\tau_{\rm AD}$ is taken to be $10t_{\rm ff}$. For these models (see § 5), with $\rho_0 = 2 \times 10^{-18}$ g cm^{-3}, the free-fall time $t_{\rm ff} = t_{\rm ff}(\rho_0)$ equals 1.486×10^{12} s. With $B_{oi} = 200$ μG at an initial number density of $n_0 = 6 \times 10^5$ cm^{-3}, these models start with a ratio of magnetic to gravitational energy of $\gamma_i = 0.58$ for the prolate clouds and $\gamma_i = 0.43$ for the oblate clouds with 20 : 1 initial density ratios (see § 5). For the clouds with an initial 100 : 1 density ratio, $\gamma_i = 0.81$ for the prolate clouds and $\gamma_i = 0.57$ for the oblate clouds. With the addition of the magnetic pressure, both the prolate and oblate clouds are initially in a quasi-equilibrium state, such that the clouds rotate for several free-fall times without collapsing or expanding significantly (Boss 1997).

There are, however, several magnetic field effects that are not treated in the simple approximations used in these models, namely, flattening along magnetic field lines and magnetic braking of rotation. The latter effect has been studied in the context of ideal MHD models by Tomisaka (2000), who found that angular momentum transport caused by magnetic tension forces during collapse led to significant loss of angular momentum, and by Burkert & Balsara (2001), who found that magnetic braking was sufficiently rapid to prevent fragmentation during the collapse of a rotating cloud that formed a wide binary in the absence of magnetic fields. Both of these studies, however, assumed flux freezing, whereas the loss of magnetic flux during ambipolar diffusion can be expected to weaken the efficiency of magnetic braking. The nonideal MHD models of Basu & Mouschovias (1994, 1995a 1995b), which included ambipolar diffusion, showed that magnetic braking is largely ineffective during the dynamic collapse phase of magnetically supercritical cores—the core's angular momentum is roughly conserved during this phase. These models suggest that the neglect of magnetic braking in the present models may not be of particular concern. Nevertheless, the validity of the approximate treatment of magnetic fields outlined in this section should be verified by subsequent calculations with a three-dimensional MHD code that also includes self-gravity and radiative transfer.

5. INITIAL CONDITIONS

Table 1 lists the initial conditions for the models described in this paper. The primary variations explored in these models are the initial degree of central concentration in the density profile, the initial shape of the cloud, and the initial rotation rate.

All clouds begin with a radial density profile, which is Gaussian, with a central density ($\rho_o = 2 \times 10^{-18}$ g cm^{-3}) chosen to be either 20 or 100 times higher than that at the boundary of the cloud (ρ_R). Initial Gaussian density profiles were originally investigated (Boss 1987) because they offered a simple way to define a cloud core with a density profile intermediate between the two extremes that had been used previously: the singular isothermal sphere (Shu 1977) and the uniform density cloud. In addition, the Gaussian density profile is similar to that of the Bonnor-Ebert sphere, which is an equilibrium state for an isothermal cloud. Gaussian profiles appear to be necessary for reproducing binary properties such as the mass ratio distribution (Bate 2000). Observations since 1987 have shown that the Gaussian profile is a reasonable approximation for precollapse clouds (e.g., Ward-Thompson, Motte, & André 1999; André, Ward-Thompson, & Barsony 2000), although the Bonnor-Ebert sphere may be superior (Alves, Lada, & Lada 2001). Note that because the initial density profiles are truncated by the edge of the grid, at a point where the density has fallen to 0.05 or 0.01 of that at the center of the cloud, the rapid decrease in density that would occur in a Gaussian profile at very large radii does not occur in these models.

Initially, the clouds are either prolate or oblate (Myers et al. 1991; Jones, Basu, & Dubinski 2001; Curry & Stahler 2001), with an axis ratio of 2 : 1 and with a random pattern of noise added to the density distribution at the 10% level. No other perturbations are added to induce fragmentation. With a cloud radius of $R = 1.0 \times 10^{17}$ cm and a temperature of 10 K, the initial ratio of thermal to gravitational energy is $\alpha_i = 0.39$ for the prolate clouds and 0.30 for the oblate clouds with the 20 : 1 initial density ratio, and $\alpha_i = 0.55$ for the prolate clouds and 0.39 for the oblate clouds with the 100 : 1 initial density ratio. These ratios are to be compared to the ratios of magnetic to gravitational energy of $\gamma_i = 0.58$ for the prolate clouds and 0.43 for the oblate clouds with 20 : 1 density ratios, and $\gamma_i = 0.81$ for the prolate clouds and 0.57 for the oblate clouds with 100 : 1 density ratios. Evidently, the magnetic support initially dominates the thermal support for all of these cloud models. The cloud masses are 1.5 and 2.1 $M_\odot$, respectively, for the prolate and oblate clouds with a 20 : 1 density ratio, and 0.96 and 1.5 $M_\odot$, respectively, for the prolate and oblate clouds with a 100 : 1 density ratio.

An initial solid body rotation rate ranging from 10^{-14} to 10^{-13} rad s^{-1} around the short axis of the clouds leads to initial ratios of rotational to gravitational energy varying from $\beta_i = 1.2 \times 10^{-4}$ to 0.015 for the prolate clouds and from $\beta_i = 1.1 \times 10^{-4}$ to 0.013 for the oblate clouds. This range of initial rotation rates and rotational energies is comparable to that inferred for many dense molecular cloud cores (Goodman et al. 1993), although some clouds exhibit evidence for even higher rotation rates.

6. RESULTS

Table 1 displays the initial conditions and basic results for 16 models with the standard numerical resolution of $N_r = 200$, $N_\theta = 22$ (with reflection symmetry through the midplane), $N_\phi = 128$ (with π symmetry), and $N_{lm} = 16$. With these symmetry assumptions, the resolution is equivalent to a total of over 1,000,000 grid points. The standard resolution should be sufficient to satisfy the four Jeans conditions for a spherical coordinate grid (Boss et al. 2000) and

TABLE 1
INITIAL CONDITIONS AND RESULTS FOR THE MODELS

Model	Geometry	ρ_o/ρ_R	Ω_i	β_i	$t_f/t_{\rm ff}$	$\rho_{\rm max}$	d/AU	Result
P2A.....	Prolate	20:1	1.0×10^{-13}	0.012	5.024	1.4×10^{-10}	1.8	bin
P2B.....	Prolate	20:1	8.1×10^{-14}	0.0080	5.146	3.8×10^{-12}	53	bin
P2C.....	Prolate	20:1	5.5×10^{-14}	0.0037	5.129	2.9×10^{-12}	40	bin
P2D	Prolate	20:1	3.2×10^{-14}	0.0013	5.107	2.4×10^{-11}	17	bin
P2E.....	Prolate	20:1	1.0×10^{-14}	0.00012	5.068	8.8×10^{-11}	3.5	bin
O2A.....	Oblate	20:1	1.0×10^{-13}	0.011	2.760	1.0×10^{-10}	20	ring
O2B	Oblate	20:1	8.1×10^{-14}	0.0070	2.835	7.0×10^{-11}	27	ring
O2C	Oblate	20:1	5.5×10^{-14}	0.0032	2.794	3.2×10^{-11}	13	ring
O2D.....	Oblate	20:1	3.2×10^{-14}	0.0011	2.644	1.1×10^{-10}	8.0	quad
O2E	Oblate	20:1	1.0×10^{-14}	0.00011	2.615	7.4×10^{-10}	2.3	quad
P1A.....	Prolate	100:1	1.0×10^{-13}	0.015	9.523	1.0×10^{-11}	6.7	bin
P1B.....	Prolate	100:1	8.1×10^{-14}	0.010	9.522	7.2×10^{-9}	0.23	bin
P1C.....	Prolate	100:1	5.5×10^{-14}	0.0047	9.585	1.9×10^{-9}	1.9	bin
P1D	Prolate	100:1	3.2×10^{-14}	0.0016	9.295	5.7×10^{-11}	1.3	bin
P1E.....	Prolate	100:1	1.0×10^{-14}	0.00015	9.257	7.8×10^{-10}	1.3	bin
O1A.....	Oblate	100:1	1.0×10^{-13}	0.013	5.282	4.9×10^{-12}	40	ring
O1B	Oblate	100:1	8.1×10^{-14}	0.0088	5.187	5.0×10^{-12}	45	ring
O1C.....	Oblate	100:1	5.5×10^{-14}	0.0040	5.080	9.1×10^{-12}	20	quad
O1D.....	Oblate	100:1	3.2×10^{-14}	0.0013	5.023	1.0×10^{-11}	19	ring
O1E	Oblate	100:1	1.0×10^{-14}	0.00013	4.964	2.4×10^{-10}	6.7	quad

NOTE.—Units for Ω_i and $\rho_{\rm max}$ are rad s^{-1} and g cm^{-3}, respectively. For results, bin means the outcome is a binary system, ring is a ring system, and quad is a quadruple system.

thus enable a physically reasonable solution, although the Jeans conditions are checked explicitly (as described below) throughout the runs, and models with increased spatial resolution have been run to further support the results of the standard resolution models (Boss 2000).

The first five columns in Table 1 note whether the initial cloud started with a prolate or oblate shape, the initial density contrast between the center and boundary of the cloud, the initial rotation rate, and the initial ratio of rotational to gravitational energy. The last four columns give the results: the final time achieved (in units of the free-fall time); the maximum density in the midplane at that time; the diameter of the binary, multiple, or ring system that results; and a classification of the outcome into a binary (bin), ring, or quadruple (quad) system.

6.1. *Prolate Clouds*

We begin with an examination of a typical prolate cloud model, model P2B. As seen in Figure 1, this model spends several free-fall times supported by the initial magnetic field pressure, and only after $\sim 4 t_{\rm ff}$ has sufficient ambipolar diffusion occurred for the cloud to begin to contract appreciably toward its center. By $\sim 5 t_{\rm ff}$ (Fig. 1*c*), the center of the cloud is in rapid dynamic collapse. Note that the cloud retains a memory of its initially prolate shape throughout these early phases. Shortly after $5.141 t_{\rm ff}$, the cloud fragments into two clumps (Fig. 1*d*) as a result of its initial prolate shape.

Figure 2 presents a more detailed look at the binary protostar that forms in model P2B. The binary clumps continue to become better defined (Fig. 2*a*). The temperature contours (Fig. 2*b*) show that while most of the central region of the protostar has been heated by compressional energy to temperatures of the order of 20 K, the narrow region between the binary clumps has cooled back down to the initial value of 10 K because of the decompressional cooling associated with the rebound away from the center and toward the clumps, as seen in the velocity vectors plot (Fig. 2*c*). The infalling gas from the rest of the cloud is infalling onto the clumps with speeds on the order of 1 km s^{-1} at this early phase.

Figure 2*d* shows that the calculation of model P2B obeys the Jeans length conditions (Truelove et al. 1997; Boss et al. 2000) that the four grid spacings associated with a spherical coordinate hydrodynamics code remain smaller than $\lambda_{\rm J}/4$ throughout the evolution if spurious fragmentation is to be avoided. Here the local Jeans length is defined as $\lambda_{\rm J} = (\pi c_s^2/G\rho)^{1/2}$, where c_s is the local isothermal sound speed, G is the gravitational constant, and ρ is the local density. For a spherical coordinate grid, each linear grid spacing must remain less than $\lambda_{\rm J}/4$, as well as $\Delta x = (\Delta x_r \Delta x_\phi \Delta x_\theta)^{1/3}$ (Boss et al. 2000). While not sufficient to ensure accuracy, the Jeans conditions appear to be necessary in general for a physically realistic calculation of fragmentation. Figure 2*d* shows that toward the end of the calculation, the Jeans length becomes so small that with the present grid structure (cf. the fully adaptive mesh employed by Truelove et al. 1997), it is increasingly difficult to continue the calculation while still obeying the Jeans conditions. In practice, reaching this point represents the end of the calculation. Further subfragmentation might occur during the subsequent contraction of the prolate cloud, but a more adaptive mesh structure would be required.

Figure 3 presents cross sections through the center of one of the binary clumps for model P2B (note that by the assumed π-symmetry assumption, the two clumps are identical). Figure 3*a* shows that the clump is fairly spherical and not all that flattened into the midplane. The temperature contours in Figure 3*b* are similarly nonflattened. The velocity vectors show that gas that infalls down the rotation axis bounces away from the center and flows outward onto the clump, where it meets gas infalling directly onto the clump from the rest of the cloud. The region where the velocity vectors converge, just inward of the density maximum in the

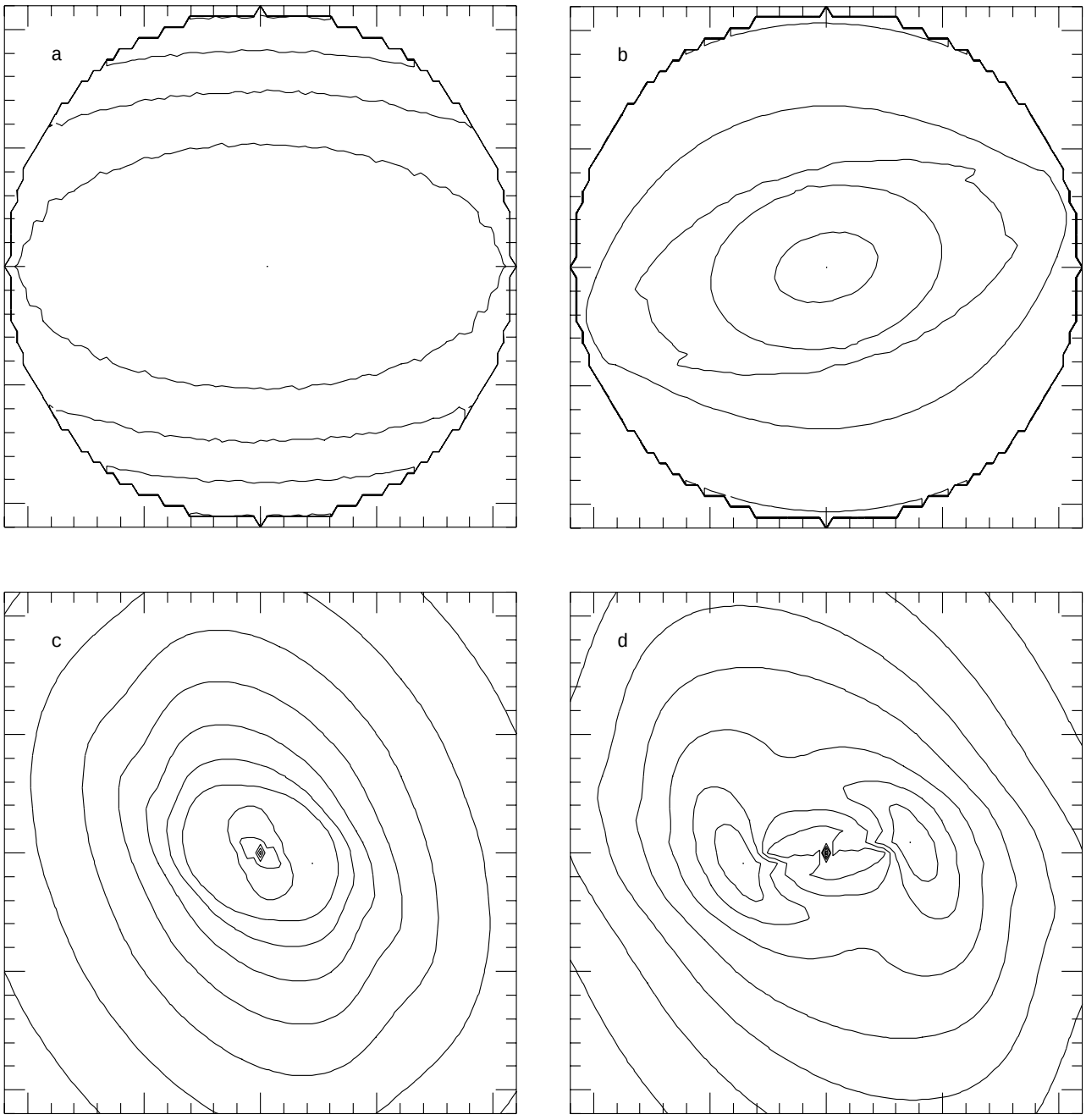

FIG. 1.—Evolution of the midplane density contours for an initially prolate, rotating, magnetic cloud core (model P2B) shown at four times: (*a*) $t = 0.0t_{\rm ff}$, $\rho_{\rm max} = 2.0 \times 10^{-18}$ g cm^{-3}, box radius $= 1.0 \times 10^{17}$ cm; (*b*) $t = 3.702t_{\rm ff}$, $\rho_{\rm max} = 1.0 \times 10^{-17}$ g cm^{-3}, box radius $= 1.0 \times 10^{17}$ cm; (*c*) $t = 5.141t_{\rm ff}$, $\rho_{\rm max} = 4.0 \times 10^{-14}$ g cm^{-3}, box radius $= 3.0 \times 10^{15}$ cm; (*d*) $t = 5.145t_{\rm ff}$, $\rho_{\rm max} = 4.0 \times 10^{-13}$ g cm^{-3}, box radius $= 1.2 \times 10^{15}$ cm. Contours represent factors of 2 change in density. A binary protostar forms: two density maxima orbit around a central density minimum in (*d*).

clump, is the region of maximum compression and thus has the highest temperatures. Note that the thin-disk approximation was used for the magnetic tension force in these models, whereas the configuration shown in Figure 3 is not thin, at least not locally. This fact is clearly a drawback of the somewhat crude approximations used in these models: if initially straight magnetic fields had been included in a rigorously correct manner, they would have forced the collapsing cloud into a thin disk all by themselves, even without significant rotation.

The binary clumps that form in model P2B have masses of about 0.005 $M_\odot \sim 5\ M_{\rm Jup}$ at the time shown in Figure 2, where all adjacent gas with a density at least 0.1 that of the density maximum is included in the clump. The ratio of thermal to gravitational energy in the clumps is about 0.4, and the ratio of rotational to gravitational energy is about 0.3; i.e., the clumps are rotating quite rapidly and are gravitationally bound. While the subsequent survival of the clumps cannot be assured in the absence of further calculations, they appear to be likely to continue along the path toward becoming protostars.

Table 1 summarizes the results for the prolate clouds with varied initial rotation rates, showing that for all five of these relatively slowly rotating clouds, the result is the same: fragmentation into a binary protostar system, with an initial separation ranging from about 2 to 50 AU. When the initial

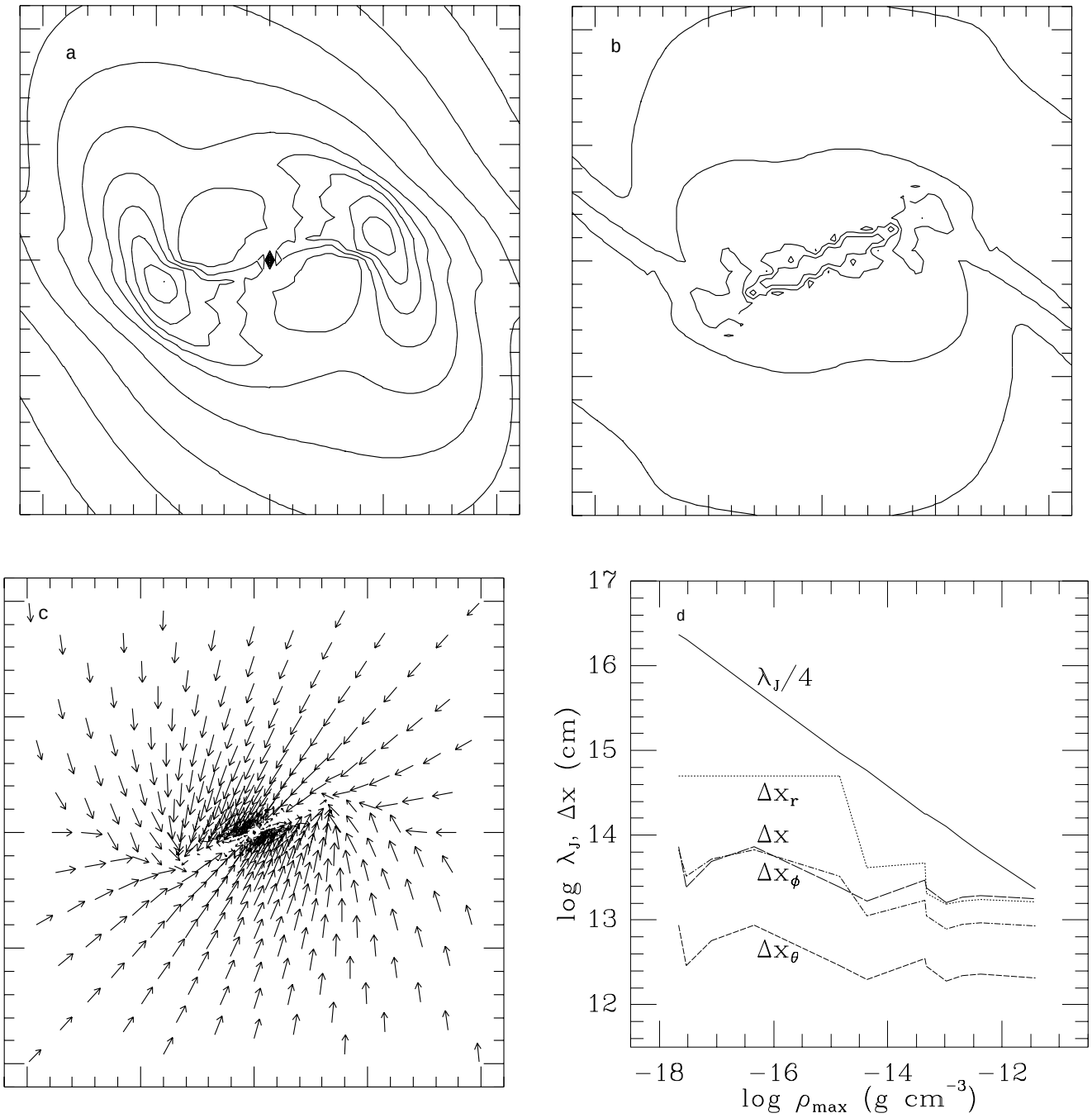

FIG. 2.—Details of the binary protostar shown in Fig. 1 for model P2B, with (*a*), (*b*), and (*c*) at a time of $t = 5.146t_{\rm ff}$, shortly after the last time depicted in Fig. 1. (*a*) Midplane density contours with $\rho_{\rm max} = 4.0 \times 10^{-12}$ g cm^{-3} in the binary protostar and a density minimum at the center. (*b*) Midplane temperature contours with $T_{\rm max} = 24$ K close to the density maxima in the binary and a temperature minimum along the region linking the two density maxima. Contours represent factors of 2 change in density for (*a*) and 1.3 in temperature for (*b*). (*c*) Midplane velocity vectors with maximum velocity of 8.7×10^4 cm s^{-1} showing infall onto the binary protostar and expansion away from the center along the region linking the density maxima. Only every fourth grid point in radius and azimuth is plotted. The box radius is 8.2×10^{14} cm for (*a*), (*b*), and (*c*). (*d*) Evolution of the four spherical grid spacings compared to the Jeans length criterion (Boss et al. 2000) with increasing maximum density in the midplane throughout the evolution of model P2B. The value of each length is plotted at the position of the density maximum.

cloud is considerably more centrally concentrated initially, with a central density 100 times larger than the boundary density, the results do not change significantly: again, all five prolate clouds with varied rotation rates collapse and fragment into at least transient binary protostars, although in this case the initial separations of the binary clumps are considerably smaller than in the case of the smaller initial density concentrations, namely, about 0.2–7 AU, as expected. The timescale for collapse to begin is longer for the 100 : 1 clouds because they begin with a larger value of $\gamma_i = 0.81$. These results suggest that the choice of the initial density profile is not too critical to the outcome of the collapse and fragmentation process for magnetic clouds, provided that the initial density profile is Gaussian-like, with a nonsingular central density. As pointed out by Boss (2000), the inclusion of magnetic tension forces appears to be largely

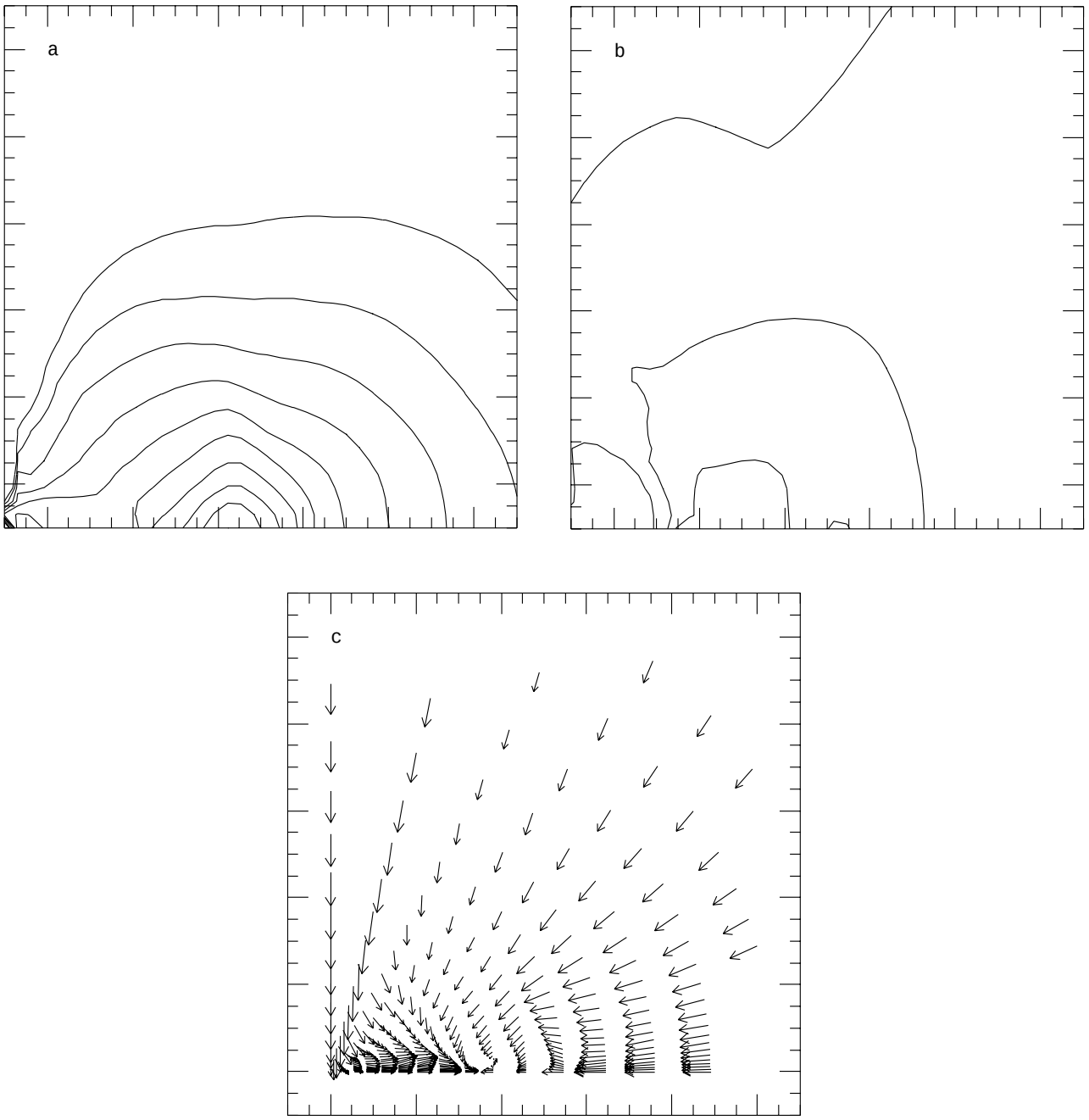

FIG. 3.—Cross sections through one of the binary clumps shown in Figs. 1 and 2 for model P2B, all at a time of $t = 5.146t_{\rm ff}$. The rotation axis forms the left-hand border for these three plots. (*a*) Azimuthal plane density contours with $\rho_{\rm max} = 4.0 \times 10^{-12}$ g cm^{-3} through a binary clump, showing a density minimum at the center. (*b*) Azimuthal plane temperature contours with $T_{\rm max} = 20$ K in the binary clump and a temperature minimum at the center. Contours represent factors of 2 change in density for (*a*) and 1.3 in temperature for (*b*). (*c*) Azimuthal plane velocity vectors with maximum velocity of 9.4×10^4 cm s^{-1} showing infall onto the binary clump and expansion away from the center. Only every fourth grid point in radius is plotted. The box radius is 8.2×10^{14} cm for (*a*), (*b*), and (*c*).

responsible for the tenacity of fragmentation, even in the case of a 100 : 1 initial density concentration: magnetic tension helps to prevent a central density singularity from forming and forcing the cloud to become a single protostar.

The insensitivity of the results shown in Table 1 to the initial rotation rates shows that the fragmentation obtained in these relatively slowly rotating clouds is not strongly dependent on rotation. Hence, the neglect of magnetic braking effects in these models should not be critical to the outcome, compared to the major effect magnetic braking had in the ideal MHD models of the collapse and fragmentation of a relatively rapidly rotating cloud by Burkert & Balsara (2001).

6.2. *Oblate Clouds*

We now turn to the case of the initially oblate clouds in Table 1. Figure 4 presents the evolution of model O2D. This cloud, having a somewhat lower initial ratio of magnetic to gravitational energy than model P2B, begins a dynamic collapse phase caused by ambipolar diffusion after only a few free times: by $2.6t_{\rm ff}$ (Fig. 4*c*), the cloud has collapsed to form

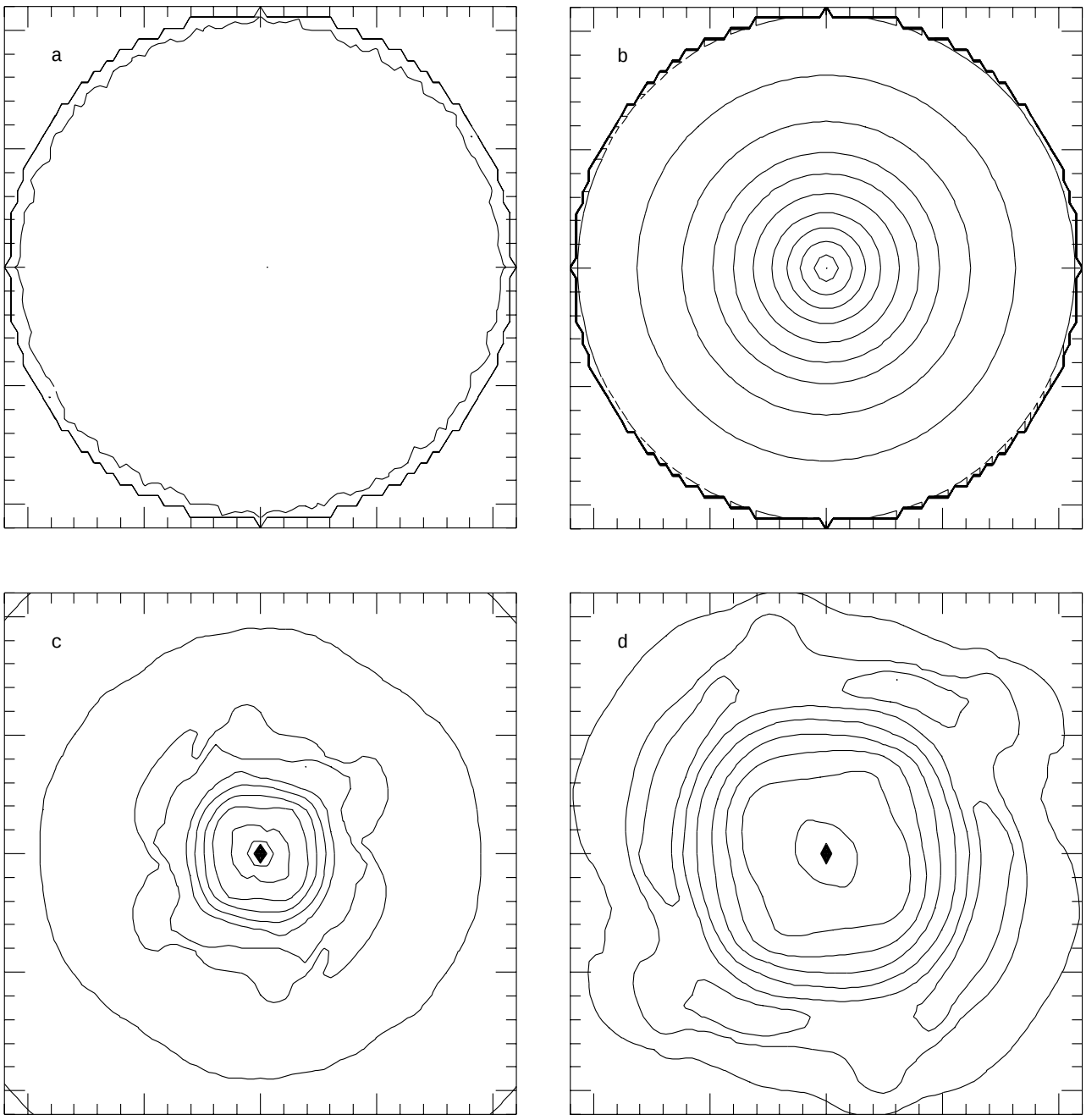

FIG. 4.—Evolution of the midplane density contours for an initially oblate, rotating, magnetic cloud core (model O2D) shown at four times: (*a*) $t = 0.0t_{\rm ff}$, $\rho_{\rm max} = 2.0 \times 10^{-18}$ g cm^{-3}, box radius $= 1.0 \times 10^{17}$ cm; (*b*) $t = 2.367t_{\rm ff}$, $\rho_{\rm max} = 1.8 \times 10^{-16}$ g cm^{-3}, box radius $= 1.0 \times 10^{17}$ cm; (*c*) $t = 2.643t_{\rm ff}$, $\rho_{\rm max} = 5.8 \times 10^{-11}$ g cm^{-3}, box radius $= 1.1 \times 10^{14}$ cm; (*d*) $t = 2.644t_{\rm ff}$, $\rho_{\rm max} = 8.4 \times 10^{-11}$ g cm^{-3}, box radius $= 6.6 \times 10^{13}$ cm. Contours represent factors of 2 change in density. A lumpy ring is evident in (*c*), orbiting around a central density minimum, and the ring begins to break up into at least four clumps in (*d*).

a relatively high density disk that rebounds at the center to form an initially nearly axisymmetric ring. Because a high-density ring is likely to be gravitationally unstable, however, nonaxisymmetry begins to grow in the ring and it fragments into four clumps by $2.644t_{\rm ff}$.

Figure 5 presents a more detailed look at the ring and clumps in model O2D at a slightly later time, when the clumps have become better defined with respect to the ring. A strong preference for fragmenting into four clumps is evident, although it must be stressed that because of the assumed symmetry, only even m modes can grow, so the formation of four rather than three or five clumps (or more) may well be a numerical artifact. Figure 5*c* shows that the clumps form on the inner edge of a region where the midplane temperature is rising toward its maximum values, i.e., in a region where both high densities and relatively moderate temperatures conspire to make fragmentation most likely. Figure 5*c* also shows that the clumps form in a region of the ring that is largely centrifugally supported, and that the central regions are strongly rebounding outward, leading to the central density and temperature minima. Figure 5*d* shows that model O2D is also well resolved with respect to the four Jeans conditions. The clumps evident in Figure 5*a* have masses of either about 0.0007 $M_\odot \sim 0.7$ $M_{\rm Jup}$, or about 0.0003 $M_\odot \sim 0.3$ $M_{\rm Jup}$ at the time shown in the figure. The significance of these extremely low initial fragment

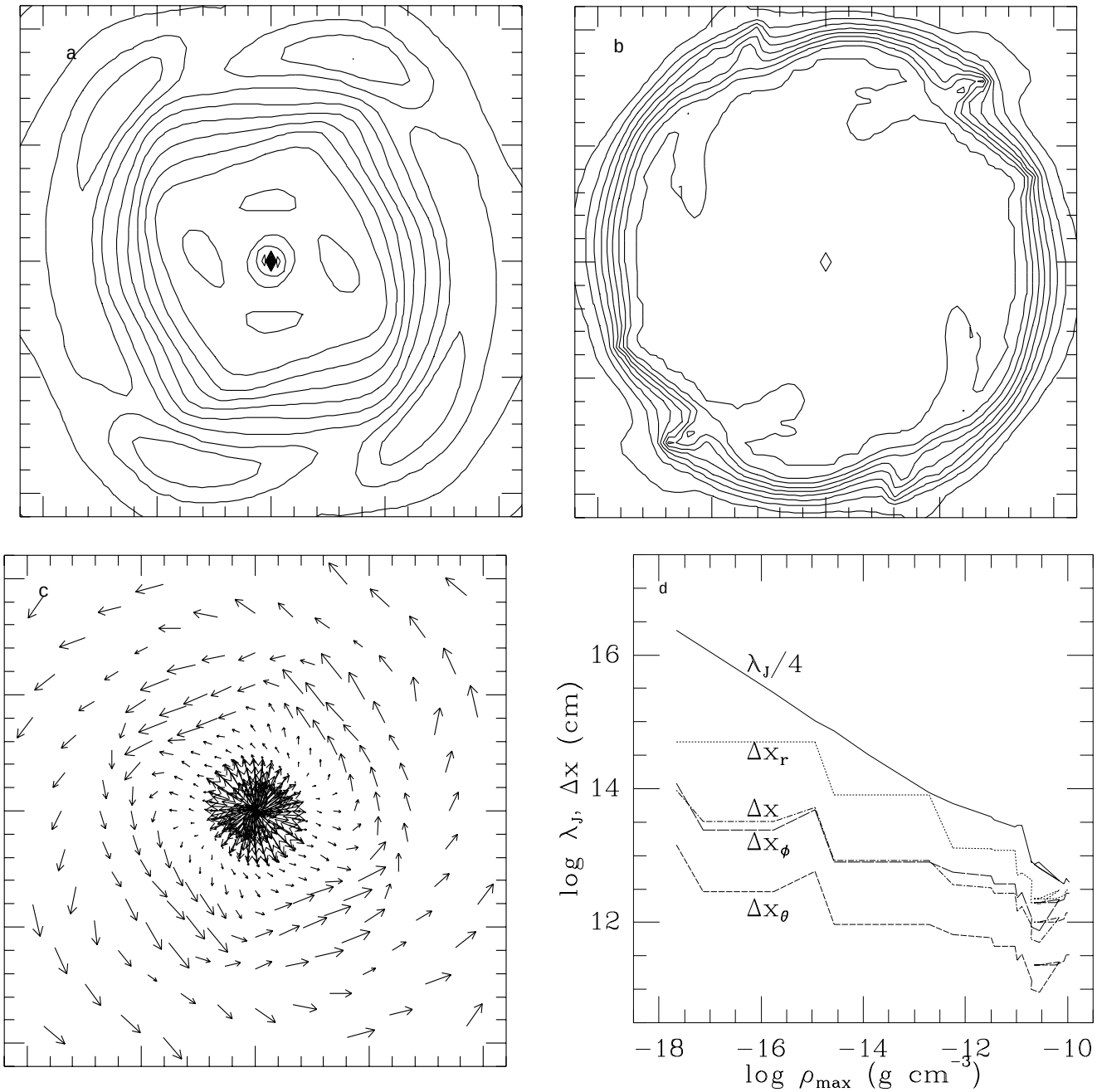

FIG. 5.—Details of the fragmenting ring system shown in Fig. 4 for model O2D, with (*a*), (*b*), and (*c*) at a time of $t = 2.645t_{\rm ff}$, shortly after the last time depicted in Fig. 4. (*a*) Midplane density contours with $\rho_{\rm max} = 1.1 \times 10^{-10}$ g cm^{-3} in the clumps in the ring with a density minimum at the center. (*b*) Midplane temperature contours with $T_{\rm max} = 79$ K in the ring and a temperature minimum at the center. Contours represent factors of 2 change in density for (*a*) and 1.3 in temperature for (*b*). (*c*) Midplane velocity vectors with maximum velocity of 8.7×10^4 cm s^{-1} showing the expansion away from the center toward the centrifugally supported ring. Only every fourth grid point in radius and azimuth is plotted. The box radius is 6.6×10^{13} cm for (*a*), (*b*), and (*c*). (*d*) Evolution of the four spherical grid spacings compared to the Jeans length criterion (Boss et al. 2000) with increasing maximum density in the midplane throughout the evolution of model O2D. The value of each length is plotted at the position of the density maximum, which varies during the central rebounds that occur at the highest densities reached.

masses was emphasized by Boss (2001); if one or two of these fragments survive subsequent evolution and are ejected outward as a result of the orbital decay of the quadruple system, they might escape the parent cloud by the time that they have acquired only planetary-type masses, in spite of having formed through the star formation process.

Table 1 summarizes the results for the oblate clouds: all five oblate clouds (O2A to O2E) with varied rotation rates collapse to form rings, and several of these rings fragment into apparent quadruple protostar systems. For three of the models, the rings that formed could not be evolved far enough in time to observe their fragmentation phase without violating the Jeans conditions, even when the models were recalculated with doubled ϕ grid resolution and with a radial grid specialized to provide uniform radial grid spacing in the center of the cloud. Given the results for the

clouds where the Jeans conditions could be satisfied to the point of fragmentation, there is little doubt that all of the rings should eventually fragment into multiple protostar systems with initial separations on the order of 2–30 AU. Table 1 also shows that even when the initial density concentration was increased from 20 : 1 to 100 : 1 (O1A to O1E), the tendency for initially oblate magnetic clouds to collapse to form rings that fragment into multiple protostar systems remains as a likely outcome. Again, the longer timescale for collapse to start (about $5t_{\rm ff}$ compared to about $3t_{\rm ff}$) is caused by the higher values of $\gamma_i = 0.57$ for the initially more centrally concentrated clouds; however, once collapse begins, the basic results are unchanged.

7. CONCLUSIONS

We have seen that magnetic fields, rather than hindering the fragmentation of dense molecular cloud cores, may actually aid in their fragmentation by helping to avoid central density singularities that would force a cloud to become a single protostar (Boss 2000). Magnetic fields may also be responsible for a central rebound that results in decompressional cooling sufficient to lower the local Jeans mass and permit clumps to form with starting masses less than 1 $M_{\rm Jup}$ (Boss 2001). Initially prolate dense cloud cores tend to remember their initial conditions and collapse to fragment into binary protostar systems, whereas initially oblate clouds, with no such preference, tend to fragment into multiple systems with four or possibly more protostars. The recent determination that the best fit for observed molecular cloud cores is a triaxial shape that is more nearly oblate than prolate (Jones, Basu, & Dubinski 2001) suggests that multiple protostellar systems may be much more frequently formed (Larson 1995; Sterzik & Durisen 1998; Reipurth 2000; Reipurth & Clarke 2001) than has usually been thought to be the case. The fragmentation of intermediate ring configurations in the oblate clouds seems to support Li's (2001) conjecture about the fragmentation of magnetically supercritical rings into multiple protostar systems. The models also seem to support the Galli et al. (2001) hypothesis that rapid loss of magnetic flux during protostellar collapse is needed in order to form binary stars.

Fragmentation thus appears to be alive and well as the leading explanation for the formation of binary and multiple-star systems, even in the presence of significant magnetic fields. Nevertheless, because these calculations are based on necessarily simple approximations regarding the physics of magnetic fields, the situation will remain unsettled until such time as a true MHD code, capable of handling self-gravity and radiative transfer, is used to study similar collapse and fragmentation problems.

The numerical calculations were performed on the Carnegie Alpha Cluster, which, along with this work, is partially supported by the National Science Foundation under grants AST 99-83530 and MRI 99-76645. I thank Gotthard Sághi-Szabó for cluster management, Sandy Keiser for workstation management, and the referee for a valuable report.

REFERENCES

Alves, J., Lada, C., & Lada, E. 2001, Nature, 409, 159
André, P., Ward-Thompson, D., & Barsony, M. 2000, in Protostars and Planets IV, ed. V. Mannings, A. P. Boss, & S. S. Russell (Tucson: Univ. Arizona Press), 59
Basu, S. 1997, ApJ, 485, 240
———. 1998, ApJ, 509, 229
Basu, S., & Mouschovias, T. Ch. 1994, ApJ, 432, 720
———. 1995a, ApJ, 452, 386
———. 1995b, ApJ, 453, 271
Bate, M. R. 2000, MNRAS, 314, 33
Benz, W. 1984, A&A, 139, 378
Bodenheimer, P., Burkert, A., Klein, R. I., & Boss, A. P. 2000, in Protostars and Planets IV, ed. V. Mannings, A. P. Boss, & S. S. Russell (Tucson: Univ. Arizona Press), 675
Boss, A. P. 1987, ApJ, 319, 149
———. 1997, ApJ, 483, 309
———. 1999, ApJ, 520, 744
———. 2000, ApJ, 545, L61
———. 2001, ApJ, 551, L167
Boss, A. P., Fisher, R. T., Klein, R. I., & McKee, C. F. 2000, ApJ, 528, 325
Boss, A. P., & Myhill, E. A. 1992, ApJS, 83, 311
Bourke, T. 2001, ApJ, 554, L91
Burkert, A., & Balsara, D. 2001, BAAS, 33, 885
Ciolek, G. E., & Mouschovias, T. Ch. 1995, ApJ, 454, 194
Crutcher, R. M. 1999, ApJ, 520, 706
Curry, C. L., & Stahler, S. W. 2001, ApJ, 555, 160
Desch, S. J., & Mouschovias, T. Ch. 2001, ApJ, 550, 314
Dorfi, E. 1982, A&A, 114, 151
Duquennoy, A., & Mayor, M. 1991, A&A, 248, 485
Fiedler, R. A., & Mouschovias, T. Ch. 1993, ApJ, 415, 680
Fischer, D. A., & Marcy, G. W. 1992, ApJ, 396, 178
Fuller, G. A., Ladd, E. F., & Hodapp, K.-W. 1996, ApJ, 463, L97
Galli, D., Shu, F. H., Laughlin, G., & Lizano, S. 2001, ApJ, 551, 367
Ghez, A. M., McCarthy, D. W., Patience, J. L., & Beck, T. L. 1997, ApJ, 481, 378
Goodman, A. A., Benson, P. J., Fuller, G. A., & Myers, P. C. 1993, ApJ, 406, 528
Jackson, J. D. 1962, Classical Electrodynamics (New York: Wiley)
Jones, C. E., Basu, S., & Dubinski, J. 2001, ApJ, 551, 387
Kenworthy, M., et al. 2001, ApJ, 554, L67
Köhler, R, Kunkel, M., Leinert, C., & Zinnecker, H. 2000, A&A, 356, 541
Koresko, C. D. 2000, ApJ, 531, L147
Kroupa, P., & Burkert, A. 2001, ApJ, 555, 945
Larson, R. B. 1995, MNRAS, 272, 213
Li, Z.-Y. 2001, ApJ, 556, 813
Mathieu, R. D. 1994, ARA&A, 32, 465
Moriarty-Schieven, G. H., Powers, J. A., Butner, H. M., Wannier, P. G., & Keene, J. 2000, ApJ, 533, L143
Mouschovias, T. Ch. 1991, ApJ, 373, 169
Myers, P. C., Fuller, G. A., Goodman, A. A., & Benson, P. J. 1991, ApJ, 376, 561
Myhill, E. A., & Boss, A. P. 1993, ApJS, 89, 345
Nakamura, F., & Hanawa, T. 1997, ApJ, 480, 701
Ostriker, E. C., Stone, J. M., & Gammie, C. F. 2001, ApJ, 546, 980
Phillips, G. J. 1986a, MNRAS, 221, 571
———. 1986b, MNRAS, 222, 111
Reipurth, B. 2000, AJ, 120, 3177
Reipurth, B., & Clarke, C. 2001, AJ, 122, 432
Ressler, M. E., & Barsony, M. 2001, AJ, 121, 1098
Rodríguez, L. F., et al. 1998, Nature, 395, 355
Shu, F. H. 1977, ApJ, 214, 488
Shu, F. H., Adams, F. C., & Lizano, S. 1987, ARA&A, 25, 23
Shu, F. H., & Li, Z.-Y. 1997, ApJ, 475, 251
Smith, K. W., Bonnell, I. A., Emerson, J. P., & Jenness, T. 2000, MNRAS, 319, 991
Sterzik, M. F., & Durisen, R. H. 1998, A&A, 339, 95
Stone, J. M., & Norman, M. L. 1992, ApJS, 80, 791
Tomisaka, K. 2000, ApJ, 528, L41
Truelove, J. K., Klein, R. I., McKee, C. F., Holliman, J. H., II, Howell, L. H., & Greenough, J. A. 1997, ApJ, 489, L179
Ward-Thompson, D., Motte, F., & André, P. 1999, MNRAS, 305, 143
White, R. J., & Ghez, A. M. 2001, ApJ, 556, 265